ACS APPLIED MATERIALS & INTERFACES

Research Article

www.acsami.org

Vanadium Sulfide on Reduced Graphene Oxide Layer as a Promising Anode for Sodium Ion Battery

Ruimin Sun, Qiulong Wei, Qidong Li, Wen Luo, Qinyou An, Jinzhi Sheng, Di Wang, Wei Chen,* and Liqiang Mai*

State Key Laboratory of Advanced Technology for Materials Synthesis and Processing, Wuhan University of Technology, Wuhan 430070 China

Supporting Information

ABSTRACT: As an alternative system of rechargeable lithium ion batteries, sodium ion batteries revitalize researchers' interest due to the low cost, abundant sodium resources, and similar storage mechanism to lithium ion batteries. VS_4 has emerged as a promising anode material for SIBs due to low cost and its unique linear chains structure that can offer potential sites for sodium storage. Herein, we present the growth of VS_4 on reduced graphene oxide (rGO) as SIBs anode for the first time. The VS_4/rGO anode exhibits promising performance in SIBs. It delivers a reversible capacity of 362 mAh g^{-1} at 100 mA g^{-1} and a good rate performance. We also investigate the sodium storage behavior of the VS_4/rGO. Different than most transition metal sulfides, the VS_4/rGO composite experiences a three-step separation mechanism during the sodiation process (VS_4 to metallic V and Na_2S, then the electrochemical mechanism is akin to Na−S). The VS_4/rGO composite proves to be a promising material for rechargeable SIBs.

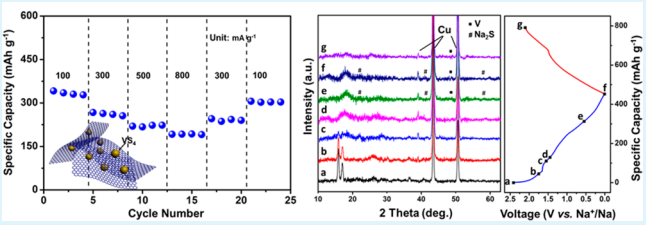

KEYWORDS: *sodium ion battery, VS_4, reduced graphene oxide, anode, energy storage*

INTRODUCTION

Rechargeable lithium ion batteries (LIBs) have been developed rapidly in the past decades and applied in portable electric devices and electric vehicles because of their high energy density and long cycling stability.[1−4] The main concern about LIBs lies in the limited resources of lithium and the rising price.[5−8] As an alternative element, sodium is the fifth most abundant element in earth's crust and the second-lightest metal compared to lithium. Room temperature sodium ion batteries (SIBs) attract much attention and show potential applications in large-scale energy storage systems (ESSs).[9−12] Many investigations on SIBs mainly focused on cathode materials, such as $Na_3V_2(PO_4)_3$,[13,14] $Na_{1.25}V_3O_8$,[15] $NaCrO_2$,[16] P2-type $Na_x[Fe_{1/2}Mn_{1/2}]O_2$,[17] $Li_{1+x}(Mn_{1/3}Ni_{1/3}Fe_{1/3})O_2$,[18] Na_xMnO_2,[19] and so on. For the anode of SIBs, the commercial graphite is not thermodynamically favorable for SIBs (a capacity of 372 mAh g^{-1} in LIBs, but less than 35 mAh g^{-1} in SIBs).[20] In addition, most intercalation/deintercalation type anodes often display low capacity.[21] Thus, developing proper anode materials with high capacity remains a desperate urgency for SIBs.

Recently, transition metal sulfides with S_2^{2-} dimers have received much attention owing to their unique physical and chemical properties. A variety of their practical applications appear, including catalysis,[22] light harvesting,[23] energy storage,[24−27] etc. For instance, iron pyrite FeS_2 is widely studied in energy-related applications about batteries.[28,29] Chen and coworkers employed pyrite FeS_2 as anode both for LIBs and SIBs, which exhibited excellent electrochemical performance.[30,31] VS_4, one of these transition metal sulfides, was found first in nature in 1906[32] and its crystal structure was established in 1964.[33] The VS_4 can be described as $V^{4+}(S_2^{2-})_2$. It is a linear-chain compound, comprising S_2^{2-} dimer connecting with the adjacent two V atoms (Figure 1). VS_4 has unique structure with weak interchain van der Waals force, which provides a loosely stacked framework. The interchain distance of VS_4 is 0.583 nm, which is much larger than the ionic diameter of Na^+ (0.196 nm). The large open channels between and in the chains offer potential sites for alkali metals diffusion and storage. In addition to being cheap and source abundant, vanadium sulfide has great

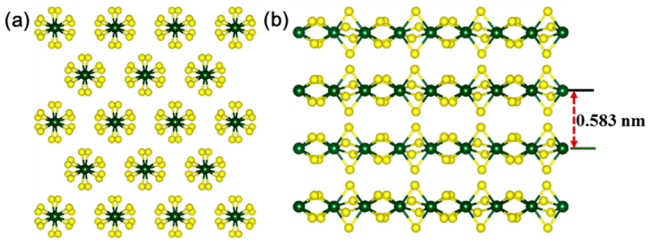

Figure 1. Structure of VS_4. (a) Repeating unit of the 1D chain structure of VS_4 (top) and (b) side-view image of monoclinic VS_4. The green balls are V atoms, and the yellow-green balls are S atoms.

Received: July 15, 2015
Accepted: September 2, 2015
Published: September 2, 2015

DOI: 10.1021/acsami.5b06385
ACS Appl. Mater. Interfaces 2015, 7, 20902−20908

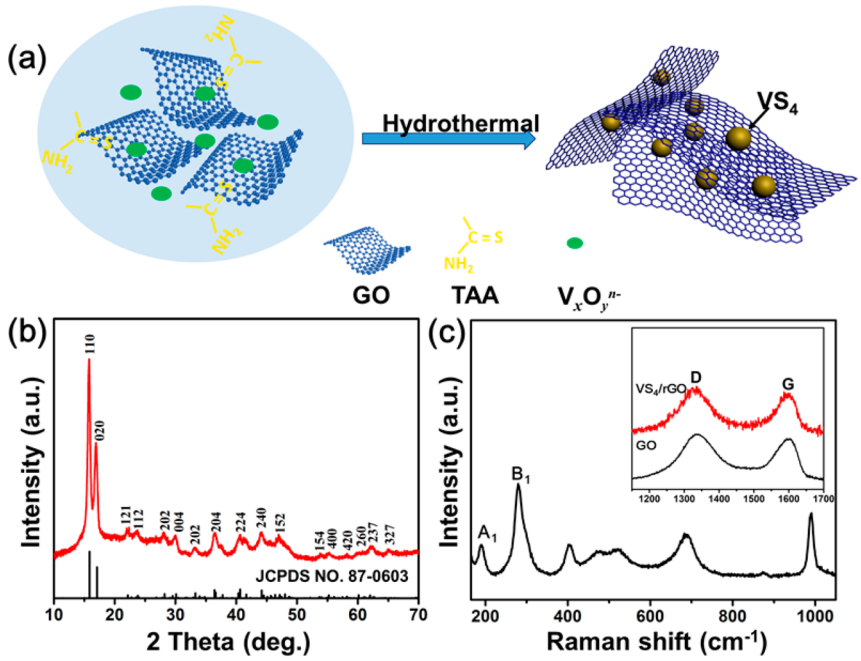

Figure 2. (a) Schematic illustration of the formation of VS_4/rGO composite. (b) XRD pattern of VS_4/rGO composite. (c) Raman spectrum of the VS_4/rGO composite and corresponding Raman spectra of the GO and VS_4/rGO (inset), respectively.

superiority for practical energy storage applications. However, there are only a few reports about this material, owing to the complex nature of the vanadium−sulfide system and the difficult synthesis of the pure VS_4 phase. Recently, Chandra et al. successfully synthesized VS_4.[34] When applied as LIBs anode, the composite exhibited excellent electrochemical performance.[34,35] It is assumed that the VS_4 is also a promising anode for SIBs. However, to the best of our knowledge, there are rare reports of applying this material as an anode for SIBs. Therefore, it is challenging but desirable to investigate this low cost material as an anode for the large-scale rechargeable SIBs.

Herein, we report VS_4/rGO composite as a new anode for SIBs. It shows superior electrochemical performance with little capacity fading over 50 cycles (~241 mAh g^{-1} at 100 mA g^{-1} after 50 cycles). The discharge capacity of 286 mAh g^{-1} can be obtained even at the high rate of 500 mA g^{-1}. Furthermore, based on the *ex situ* X-ray diffraction (XRD) analysis, energy dispersive spectroscopy (EDS) and transmission electron microscopy (TEM) analysis, the proper sodium storage mechanism is also explored.

EXPERIMENTAL SECTION

Synthesis of GO. A total of 1 g of graphite flakes were mixed with 23 mL of concentrated sulfuric acid in a 250 mL conical flask and stirred at room temperature for 24 h. Then the conical flask was placed in 40 °C water bath and 0.1 g of $NaNO_3$ was added to the suspension to be fully dissolved. After that, 1.5 g of $KMnO_4$ was slowly added to the suspension while the temperature was kept constant at about 45 °C for 30 min. Then 5 mL of deionized (DI) water was slowly added to the suspension and stirred for 5 min. Then, 40 mL of water was added to the suspension for another 15 min. After that, the conical flask was removed from water bath. The suspension was diluted by 140 mL of DI water, and then 10 mL of 30% H_2O_2 was added to reduce the unreacted $KMnO_4$. Finally, the resulting suspension was centrifuged several times to remove the unreacted acids and salts. The purified GO was dispersed in DI water by sonication for 1 h. Then the GO dispersion was subjected to another centrifugation to remove the unexfoliated GO and a brown homogeneous solution was obtained.

VS_4/rGO Preparation. A VS_4/rGO composite was prepared using a similar synthesis procedure as reported in previous paper.[34] To synthesize the VS_4/rGO composite, 3 mmol sodium metavandate ($NaVO_3$) and 6 mmol sodium hydroxide (NaOH) were dissolved in 30 mL of GO (1.5 mg/mL). Meanwhile, 15 mmol thiacetamide (TAA) was dissolved in 10 mL of GO. The as-obtained suspensions were mixed sequentially with continuous stirring. The final suspension stirred for 1 h to become homogeneous and then transferred to a 50 mL Teflon-lined autoclave, tightly sealed, and heated at 160 °C for 24 h. After cooling to room temperature, the black product was centrifugated and washed with DI water several times and dried in a vacuum oven at 60 °C for 10 h.

Material Characterizations. XRD pattern for the sample was collected by using a D8 Advance X-ray diffractometer with Cu Ka X-ray source at room temperature. Field-emission scanning electron microscopy (FESEM) images were collected with a JEOL-7100F microscope. TEM and high-resolution TEM (HRTEM) images were recorded using a JEM-2100F STEM/EDS microscope. Raman spectra were obtained using a Renishaw INVIA micro-Raman spectroscopy system. The carbon content was measured by elemental analysis (CHNS).

Electrochemical Measurements. The electrochemical properties were measured by assembling 2016 coin cells in an argon-filled glovebox. Sodium disks were used as the counter and reference electrodes. The working electrodes were fabricated on Cu foil current collectors, the slurry was obtained by mixing the as-synthesized materials, acetylene black and carboxyl methyl cellulose (CMC) binder in a weight ratio of 7:2:1. The mass loading of the electrode was 1.2−1.5 mg cm^{-2}. The electrolyte was composed of 1 M $NaClO_4$ dissolved in dimethyl carbonate (DMC)/ethylene carbon (EC) with a volume ratio of 1:1. Galvanostatic charge−discharge measurements were performed over a potential range of 0.01−2.2 V vs Na^+/Na by using a multichannel battery testing system (LAND CT2001A). Cyclic voltammetry (CV) was tested by an electrochemical workstation (CHI 760D). Electrochemical impedance spectroscopy (EIS) was tested with Autolab Potentiostat Galvanostat (PGSTAT302N). All of the measurements were carried out at room temperature.

DOI: 10.1021/acsami.5b06385
ACS Appl. Mater. Interfaces 2015, 7, 20902−20908

RESULTS AND DISCUSSION

Figure 2a illustrates the schematical synthesis process. As a reactant, C_2H_5NS (TAA) not only plays the role of a reducing agent but a sulfur donor. During the hydrothermal process, hydrolysis of C_2H_5NS releases S^{2-} under alkaline conditions. The connection between V and O in solution can be expressed as $V_xO_y^{n-}$.[36] The reaction between the reactants results in the conversion of $V_xO_y^{n-}$ to VS_4 while the GO is partially reduced to rGO, as shown in Figure 2a. XRD measurement is performed to identify the crystallographic structure and crystallinity (Figure 2b). XRD pattern of the product shows the formation of the body-centered monoclinic VS_4 phase (space group: *I2/c*) with lattice constants a = 6.77 Å, b = 10.42 Å, c = 12.11 Å (JCPDS No. 87−0603). No peaks of any other phases are detected, indicating the high phase purity. Raman spectrum (Figure 2c) of VS_4/rGO composite is obtained, bands located at 190 and 279 cm^{-1} correspond to the stretching (A_1) and bending (B_1) modes of V−S, respectively.[32] To investigate the nature of graphene in the sample, Raman spectra (inset of Figure 2c) of both GO and the VS_4/rGO composite are recorded. Typical peaks located at around 1330 and 1590 cm^{-1} are attributed to the D and G bands of the graphene, respectively. The D band is associated with the defect sites and disorders, while the G band originates from bond stretching of all C sp^2 atom pairs. The I_D/I_G ratio indicates the defect degree of graphitic carbon materials.[35] Compared with GO, the I_D/I_G ratio in VS_4/rGO composite is a little higher than the former. The ratio changes from 1.11 to 1.16, indicating that the GO is partially reduced to rGO after the hydrothermal process. More local defects and disorders are formed, mainly arising from deoxygenation of GO.[37,38]

SEM (Figure 3a, S1, Supporting Information) and TEM images (Figure 3b,c) show that the VS_4 nanoparticles grow on crumpled rGO matrix. The rGO sheets provide a structure for improvement of electrical conductivity as well as the substrate for nucleation and growth of VS_4. The particle sizes are between 100 and 200 nm. As shown in TEM (Figure 3b,c), the thin crumpled graphene sheets can be clearly observed, which effectively hamper aggregation of VS_4 nanoparticles. The HRTEM image further identifies the adhesion of thin crumpled rGO and VS_4 nanoparticles (Figure 3c). The Figure 3d shows lattice spaces of around 0.56 and 0.59 nm, which are in agreement with the (110) and (002) planes of VS_4, respectively. The fast-Fourier transform (FFT) (inset of Figure 3d) corresponds to the monoclinic VS_4 phase. Elemental analysis (CHNS) method was applied to precisely determine the carbon contents of the VS_4/rGO compounds. The amount of carbon content in the composite is around 9.8% (Table S1, Supporting Information).

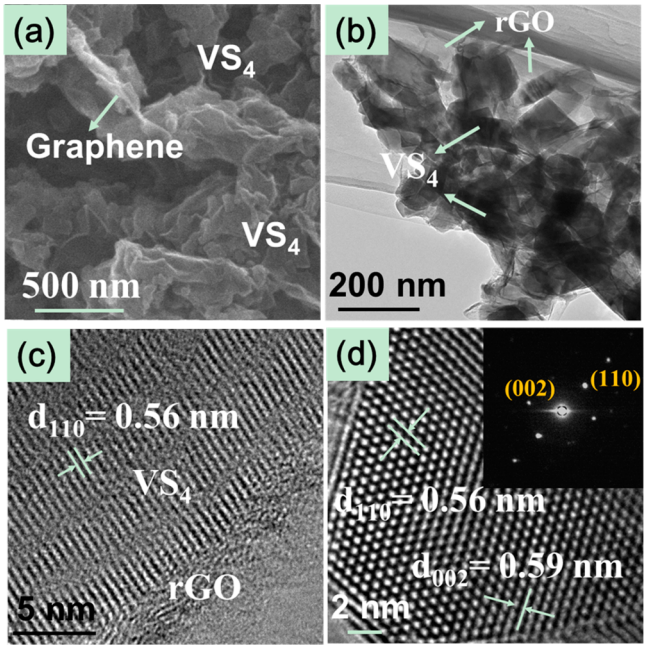

Figure 3. SEM (a) and TEM (b) images of the VS_4/rGO composite. (c) HRTEM image of VS_4/rGO composite. (d) HRTEM image of VS_4, showing the *d*-spacing of 0.56 and 0.59 nm in the (110) and (002) plane, respectively. Inset: FFT image of VS_4.

Electrochemical performance was investigated using coin cells (2016) with metallic sodium as a counter electrode. Cells were measured between 0.01 and 2.2 V vs Na^+/Na. Figure 4a shows the discharge−charge curves of the VS_4/rGO composite at the initial three cycles. The initial discharge and charge capacities are 450.4 and 338.4 mAh g^{-1}, respectively. The Coulombic efficiency (CE) of the first cycle is 75.1%. This low efficiency might attribute to inevitable electrolyte decomposition and the formation of solid electrolyte interface (SEI).[34]

Figure 4b shows the CV curve of the VS_4/rGO composite at a scan rate of 0.1 mV s^{-1}. The profile during the first cycle is different from subsequent cycles. A strong reduction peak appears at 1.6 V and disappears in the following cycles, suggesting that there is an irreversible reaction during the first discharge process. This behavior is similar to the other transition metal sulfides, such as MoS_2,[39,40] FeS_2,[41] SnS_2,[42,43] SnS,[44] etc. During the second and subsequent cycles, VS_4/rGO electrodes show reduction peaks around 0.65, 1.10, and 1.30 V versus Na^+/Na and oxidation peak around 1.50 and 1.95 V versus Na^+/Na. Two reduction peaks at 0.65 and 1.10 V represent the conversion reaction with Na. However, only one sharp oxidation peak appears at 1.50 V in the reverse oxidation process. The potential pair at 1.30/1.95 V is attributed to conversion reaction with sulfur atoms in the composite.[45] The typical peaks in the CV curves correspond well to the plateaus positions in the discharge−charge curves.

Figure 4c shows the cycling performance and CE of the composite at a current density of 100 mA g^{-1}. During the second cycle, the CE improves to 91.8%. After a few cycles, the CE of the electrode approaches 100%. The capacity of the electrode slightly decays to 287.5 mAh g^{-1} in the 15th cycle and becomes relatively stable in the further cycles. After 50 cycles, the discharge and charge capacity of VS_4/rGO are found to be 240.8 and 237.1 mAh g^{-1}, respectively. Moreover, the cycling performance of this material at high rate of 500 mA g^{-1} (Figure S2, Supporting Information) is shown; the initial discharge capacity is 285.7 mAh g^{-1}, and the capacity fades slowly. The rGO shows negligibly small contributions to the total capacity (Figure S3, Supporting Information). The main capacity is attributed to VS_4 in this composite.

Figure 4d shows the rate performance of the VS_4/rGO composite. As the current density increases from 100 to 300, 500, and 800 mA g^{-1}, the discharge capacity decreases gradually from 341.5 to 267.2, 219.9, and 192.1 mAh g^{-1}, respectively. Even suffering from rapid current density changes, the VS_4/rGO composite electrode keeps relatively stable capacity at each rate. After the high rate measurement, the current density is reduced back to 300 mA g^{-1}, and there is little capacity loss

DOI: 10.1021/acsami.5b06385
ACS Appl. Mater. Interfaces 2015, 7, 20902−20908

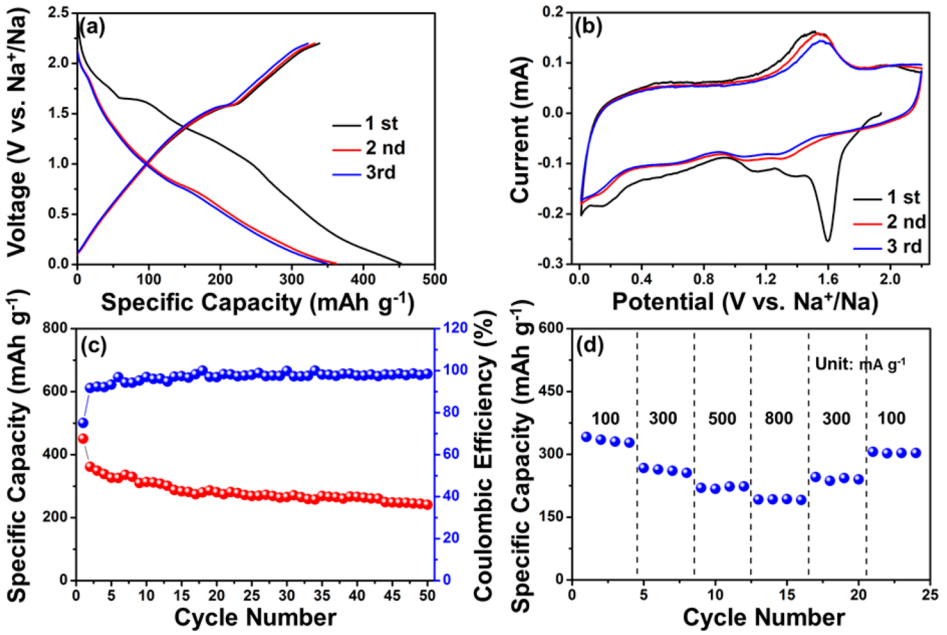

Figure 4. (a) Discharge−charge curves of the VS_4/rGO composite at the current density of 100 mA g^{-1}. (b) Cyclic voltammetry curves of VS_4/rGO composite electrode at scanning rate of 0.1 mV s^{-1}. (c) Cycling performance of VS_4/rGO composite at a current density of 100 mA g^{-1}. (d) Rate performance of VS_4/RGO composite.

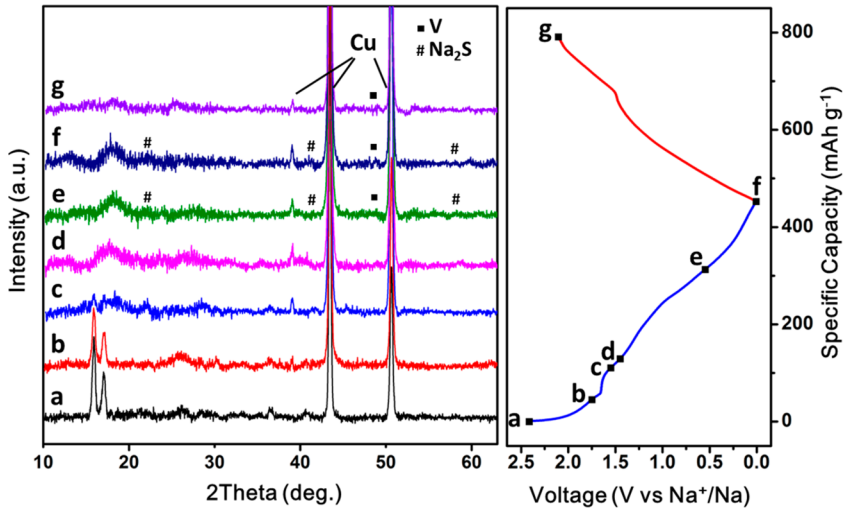

Figure 5. *Ex situ* XRD patterns of the VS_4/rGO composite collected at various voltage states as indicated in the corresponding voltage profile. (a) Pristine VS_4/rGO composite, (b−f) first discharging to 1.75, 1.55, 1.45, 0.55, and 0.01 V, respectively, and (g) first charging to 2.2 V.

with capacity retention of 93.9%, demonstrating excellent rate reversibility and stability of this VS_4/rGO composite electrode. Such an impressive electrochemical performance is attributed to the rGO dispersed between the VS_4 nanoparticles which maintains the electrical conductivity and restricts the aggregation of the nanoparticles,[34] as well as fast sodium ion diffusion from the small nanoparticles.

In order to investigate the sodium storage behavior of the VS_4/rGO composite, *ex situ* XRD analysis was carried out. XRD patterns after charging and discharging to different voltage states are shown in Figure 5. The original electrode (Figure 5a) shows a pure phase of VS_4 (JCPDS No. 87-0603) with two main peaks at 15.8° and 17.0°. When discharged to 1.75 V, there is no obvious change of the main peaks corresponding to VS_4 (Figure 5b), demonstrating no structure change at this state. The main peaks of VS_4 decrease when discharged to 1.55 V (Figure 5c), suggesting that Na insertion reaction occurs ($VS_4 + x\ Na^+ + x\ e^- \rightarrow Na_xVS_4$).[46] The two main peaks disappear after discharged to 1.45 V (Figure 5c). When continuing to discharge to 0.55 V (Figure 5d), the main peaks of VS_4 disappear thoroughly. Meanwhile, a new peak at 48.0° corresponding to the (200) peak of metallic V (JCPDS No. 01-088-2322) appears, implying that VS_4 phase has transformed to metallic V and Na_2S at this discharge stage ($Na_xVS_4 + (8 - x)\ Na^+ + (8 - x)\ e^- \rightarrow 4Na_2S + V$). The intensities of the emerging peaks increase after being fully discharged to 0.01 V (Figure 5e). When fully charged to 2.2 V (Figure 5f), the main peaks of VS_4 do not appear again, indicating an irreversible conversion reaction occurs during the first cycle. But the peak of V still exists. The following reaction can be summarized as the reaction between S and Na_2S ($Na_2S \rightarrow S + 2Na^+ + 2e^-$).[45] Although no obvious peaks of S are found in the XRD pattern,

DOI: 10.1021/acsami.5b06385
ACS Appl. Mater. Interfaces 2015, 7, 20902−20908

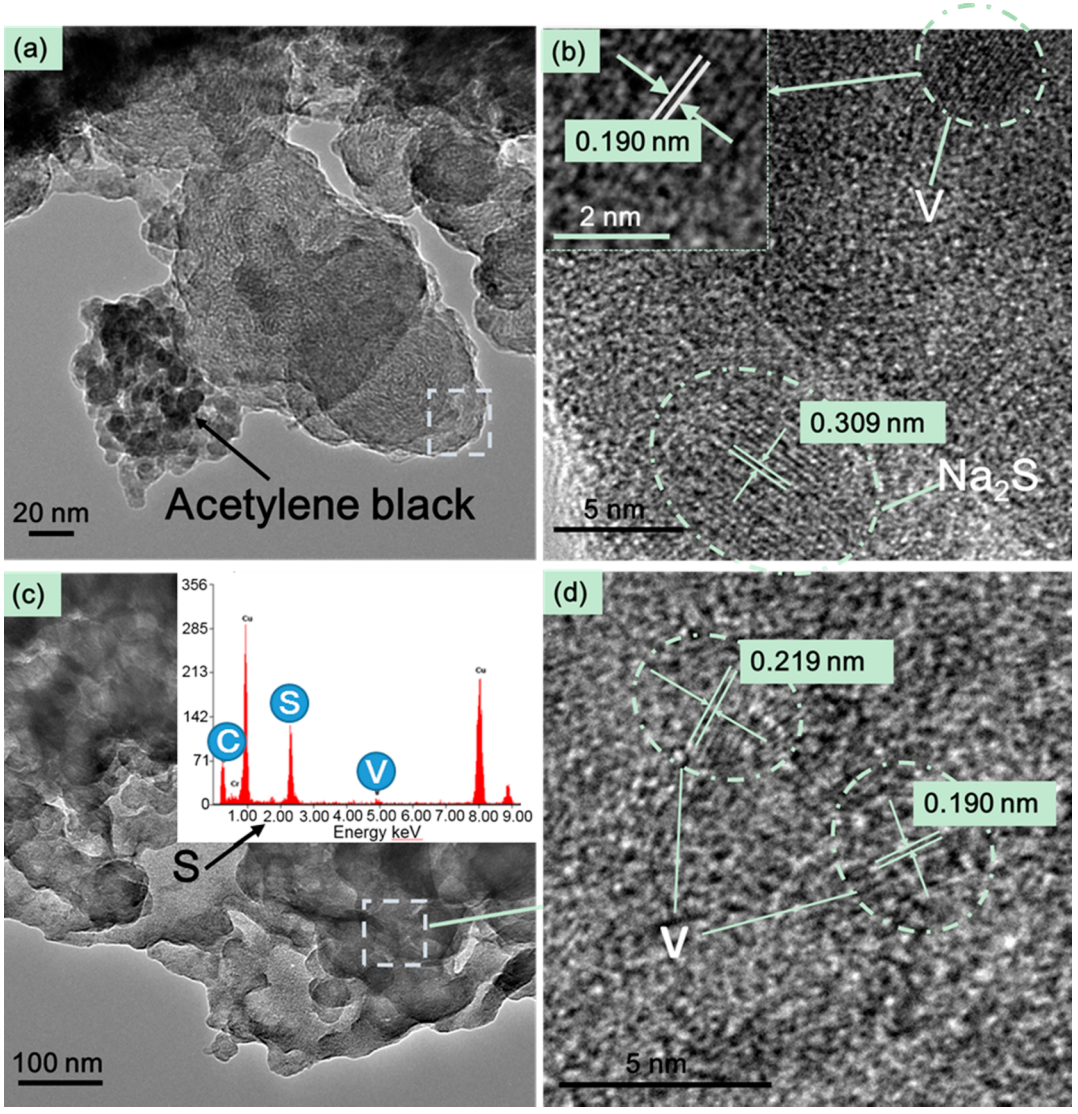

Figure 6. TEM and HRTEM images of (a,b) the fully discharged electrode (inset: enlarged HRTEM image of the V region) and (c,d) the fully charged electrode (inset: EDS spectrum, showing elemental composition of S) of VS_4/rGO at 100 mA g^{-1}.

this attributes to an amorphous S phase is formed during the charge process. The broad peak between 16−21° comes from the sample holder. (Figure S4, Supporting Information).

To further understand the mechanism of sodium storage, TEM and EDS spectra were employed to analyze the composition of the fully discharged and charged VS_4/rGO electrode. Figure 6a shows the TEM image of VS_4 after fully discharged to 0.01 V. The HRTEM image (Figure 6b) shows *d*-spacing of 0.190 nm corresponding to the (200) plane of metallic V and *d*-spacing of 0.309 nm to the Na_2S. After charged to 2.2 V, the reformation of VS_4 does not occur. HRTEM image (Figure 6d) shows *d*-spacing of 0.190 and 0.219 nm corresponding to the (200) and (111) plane of V, respectively, demonstrating that vanadium still exists in the electrode and it is inert during the charging process. The TEM (Figure 6c) and EDS spectra (inset of Figure 6c) show an S-rich region, which is in good agreement with reaction mechanism concluded from *ex situ* XRD.

Repeated generation of V during cycling is believed to improve the intrinsic electronic conductivity of the composite. To confirm this point, the electrochemical impedance (EIS) was measured for the VS_4/rGO electrode before and after cycling (Figure S5, Supporting Information). The Nyquist plots show two semicircles that are not clearly separated with a large diameter at high frequencies before cycling, indicating high interface resistance. After cycling, the depressed semicircle becomes one with a reduced diameter at high frequencies, suggesting a decreased impedance. The presence of metal vanadium after the first discharge process significantly improves the electronic conductivity of the electrode. Similar findings have been reported in MoS_2 based electrode[27] and $Ag_2V_4O_{11}$ medical cathode material.[47]

In consequence, by combining *ex situ* XRD (Figure 5) study, TEM, and EDS spectrum (Figure 6), we propose a mechanism to illustrate the discharge process of VS_4. The VS_4/rGO composite experiences a three-step separation mechanism during the sodiation process. During discharging, Na insertion reaction occurs first in the initial discharge process, follow by a conversion reaction that Na_xVS_4 decomposes to new phases of V and Na_2S. The subsequent electrochemical reaction may be attributed to the reversible conversion reaction between Na_2S and S, while metal vanadium remains inert but it improves

DOI: 10.1021/acsami.5b06385
ACS Appl. Mater. Interfaces 2015, 7, 20902−20908

conductivity of the electrode during cycling. The mechanism of conversion materials is still needed to explain in more detail.

CONCLUSIONS

In summary, we present the growth of VS_4 nanoparticles on rGO as the new anode material for SIBs. Notably, their electrochemical performance as anode for SIBs and the mechanism of sodium storage behavior during discharging and charging process are investigated systematically. The VS_4 nanoparticle and rGO in the composite are believed to function synergistically, so as to significantly stabilize electrochemical properties of the anode material. VS_4/rGO exhibits a good cycling stability and impressive high-rate capability of sodium storage. This study provides the first experimental evidence of VS_4/rGO composite electrodes as anode for electrochemical sodium storage at room temperature, and these results establish a good basis for the later research.

ASSOCIATED CONTENT

Supporting Information

The Supporting Information is available free of charge on the ACS Publications website at DOI: 10.1021/acsami.5b06385.

Additional Figures S1−S5 and Table S1. SEM image and elemental analysis (CHNS) data of VS_4/rGO composite. Cycling performance of VS_4/rGO composite at a current density of 500 mA g^{-1} and rGO at a current density of 100 mA g^{-1}. The XRD pattern of the sample holder. Nyquist plots of VS_4/rGO composite electrode before and after cycling (PDF)

AUTHOR INFORMATION

Corresponding Authors

*E-mail: mlq518@whut.edu.cn.
*E-mail: chenwei2005@whut.edu.cn.

Author Contributions

The manuscript was written through contributions of all authors. All authors have given approval to the final version of the manuscript.

Notes

The authors declare no competing financial interest.

ACKNOWLEDGMENTS

This work is supported by the National Natural Basic Research Program of China (2013CB934103 and 2012CB933003), the International Science and Technology Cooperation Program of China (2013DFA50840), the National Natural Science Fund for Distinguished Young Scholars (51425204), the National Natural Science Foundation of China (51272197), the Hubei Province Natural Science Fund for Distinguished Young Scholars (2014CFA035), the Fundamental Research Funds for the Central Universities (2013-ZD-7 and 2014-YB-001), and the Students Innovation and Entrepreneurship Training Program (WUT, 20141049701006). We are grateful to Prof. C. M. Lieber of Harvard University, Prof. J. Liu of Pacific Northwest National Laboratory and Prof. D. Y. Zhao of Fudan University for strong support and stimulating discussions.

REFERENCES

(1) Sathiya, M.; Abakumov, A. M.; Foix, D.; Rousse, G.; Ramesha, K.; Saubanère, M.; Doublet, M.; Vezin, H.; Laisa, C.; Prakash, A.; Gonbeau, D.; VanTendeloo, G.; Tarascon, J. M. Origin of Voltage Decay in High-Capacity Layered Oxide Electrodes. *Nat. Mater.* **2014**, *14*, 230−238.

(2) Armand, M.; Tarascon, J. M. Building Better Batteries. *Nature* **2008**, *451*, 652−657.

(3) Goodenough, J. B.; Park, K. S. The Li-Ion Rechargeable Battery: A Perspective. *J. Am. Chem. Soc.* **2013**, *135*, 1167−1176.

(4) An, Q.; Lv, F.; Liu, Q.; Han, C.; Zhao, K.; Sheng, J.; Wei, Q.; Yan, M.; Mai, L. Amorphous Vanadium Oxide Matrixes Supporting Hierarchical Porous Fe_3O_4/Graphene Nanowires as a High-Rate Lithium Storage Anode. *Nano Lett.* **2014**, *14*, 6250−6256.

(5) Wu, D.; Li, X.; Xu, B.; Twu, N.; Liu, L.; Ceder, G. $NaTiO_2$: A Layered Anode Material for Sodium-Ion Batteries. *Energy Environ. Sci.* **2015**, *8*, 195−202.

(6) Yabuuchi, N.; Kajiyama, M.; Iwatate, J.; Nishikawa, H.; Hitomi, S.; Okuyama, R.; Usui, R.; Yamada, Y.; Komaba, S. P2-Type $Na_x[Fe_{1/2}Mn_{1/2}]O_2$ Made from Earth-Abundant Elements for Rechargeable Na Batteries. *Nat. Mater.* **2012**, *11*, 512−517.

(7) Xie, X.; Su, D.; Chen, S.; Zhang, J.; Dou, S.; Wang, G. SnS_2 Nanoplatelet@ Graphene Nanocomposites as High-Capacity Anode Materials for Sodium-Ion Batteries. *Chem. - Asian J.* **2014**, *9*, 1611−1617.

(8) Chen, C.; Hu, P.; Hu, X.; Mei, Y.; Huang, Y. Bismuth Oxyiodide Nanosheets: A Novel High-Energy Anode Material for Lithium-Ion Batteries. *Chem. Commun.* **2015**, *51*, 2798−2801.

(9) Ong, S. P.; Chevrier, V. L.; Hautier, G.; Jain, A.; Moore, C.; Kim, S.; Ma, X.; Ceder, G. Voltage, Stability and Diffusion Barrier Differences between Sodium-Ion and Lithium-Ion Intercalation Materials. *Energy Environ. Sci.* **2011**, *4*, 3680−3688.

(10) Palomares, V.; Casas-Cabanas, M.; Castillo-Martínez, E.; Han, M. H.; Rojo, T. Update on Na-Based Battery Materials. A Growing Research Path. *Energy Environ. Sci.* **2013**, *6*, 2312−2337.

(11) Wang, L.; Lu, Y.; Liu, J.; Xu, M.; Cheng, J.; Zhang, D.; Goodenough, J. B. A Superior Low-Cost Cathode for a Na-Ion Battery. *Angew. Chem., Int. Ed.* **2013**, *52*, 1964−1967.

(12) Bommier, C.; Ji, X. Recent Development on Anodes for Na-Ion Batteries. *Isr. J. Chem.* **2015**, *55*, 486−507.

(13) Li, S.; Dong, Y.; Xu, L.; Xu, X.; He, L.; Mai, L. Effect of Carbon Matrix Dimensions on the Electrochemical Properties of $Na_3V_2(PO_4)_3$ Nanograins for High-Performance Symmetric Sodium-Ion Batteries. *Adv. Mater.* **2014**, *26*, 3545−3553.

(14) Jian, Z.; Sun, Y.; Ji, X. A New Low-Voltage Plateau of $Na_3V_2(PO_4)_3$ as an Anode For Na-Ion Batteries. *Chem. Commun.* **2015**, *51*, 6381−6383.

(15) Dong, Y.; Li, S.; Zhao, K.; Han, C.; Chen, W.; Wang, B.; Wang, L.; Xu, B.; Wei, Q.; Zhang, L.; Xu, X.; Mai, L. Hierarchical Zigzag $Na_{1.25}V_3O_8$ Nanowires with Topotactically Encoded Superior Performance for Sodium-Ion Battery Cathodes. *Energy Environ. Sci.* **2015**, *8*, 1267−1275.

(16) Kubota, K.; Ikeuchi, I.; Nakayama, T.; Takei, C.; Yabuuchi, N.; Shiiba, H.; Nakayama, M.; Komaba, S. New Insight into Structural Evolution in Layered $NaCrO_2$ during Electrochemical Sodium Extraction. *J. Phys. Chem. C* **2015**, *119*, 166−175.

(17) Pang, W. K.; Kalluri, S.; Peterson, V. K.; Sharma, N.; Kimpton, J.; Johannessen, B.; Liu, H. K.; Dou, S. X.; Guo, Z. Interplay between Electrochemistry and Phase Evolution of the P2-Type $Na_x(Fe_{1/2}Mn_{1/2})O_2$ Cathode for Use in Sodium-Ion Batteries. *Chem. Mater.* **2015**, *27*, 3150−3158.

(18) Kalluri, S.; Pang, W. K.; Seng, K. H.; Chen, Z.; Guo, Z.; Liu, H. K.; Dou, S. X. One-Dimensional Nanostructured Design of $Li_{1+x}(Mn_{1/3}Ni_{1/3}Fe_{1/3})O_2$ as a Dual Cathode for Lithium-Ion and Sodium-Ion Batteries. *J. Mater. Chem. A* **2015**, *3*, 250−257.

(19) Mendiboure, A.; Delmas, C.; Hagenmuller, P. Electrochemical Intercalation and Deintercalation of Na_xMnO_2 Bronzes. *J. Solid State Chem.* **1985**, *57*, 323−331.

(20) Chen, C.; Wen, Y.; Hu, X.; Ji, X.; Yan, M.; Mai, L.; Hu, P.; Shan, B.; Huang, Y. Na^+ Intercalation Pseudocapacitance in Graphene-Coupled Titanium Oxide Enabling Ultra-Fast Sodium Storage and Long-Term Cycling. *Nat. Commun.* **2015**, *6*, 6929−6937.

DOI: 10.1021/acsami.5b06385
ACS Appl. Mater. Interfaces 2015, 7, 20902−20908

(21) Wang, Y.; Yu, X.; Xu, S.; Bai, J.; Xiao, R.; Hu, Y. S.; Li, H.; Yang, X. Q.; Chen, L.; Huang, X. A Zero-Strain Layered Metal Oxide as the Negative Electrode for Long-Life Sodium-Ion Batteries. *Nat. Commun.* **2013**, *4*, 2365.
(22) Zhou, W.; Yin, Z.; Du, Y.; Huang, X.; Zeng, Z.; Fan, Z.; Liu, H.; Wang, J.; Zhang, H. Synthesis of Few-Layer MoS_2 Nanosheet-Coated TiO_2 Nanobelt Heterostructures for Enhanced Photocatalytic Activities. *Small* **2013**, *9*, 140−147.
(23) Ho, W.; Yu, J. C.; Lin, J.; Yu, J.; Li, P. Preparation and Photocatalytic Behavior of MoS_2 and WS_2 Nanocluster Sensitized TiO_2. *Langmuir* **2004**, *20*, 5865−5869.
(24) Feng, J.; Sun, X.; Wu, C.; Peng, L.; Lin, C.; Hu, S.; Yang, J.; Xie, Y. Metallic Few-Layered VS_2 Ultrathin Nanosheets: High Two-Dimensional Conductivity for In-Plane Supercapacitors. *J. Am. Chem. Soc.* **2011**, *133*, 17832−17838.
(25) Xu, C.; Zeng, Y.; Rui, X.; Xiao, N.; Zhu, J.; Zhang, W.; Chen, J.; Liu, W.; Tan, H.; Hng, H. H. Controlled Soft-Template Synthesis of Ultrathin C@ FeS Nanosheets with High-Li-Storage Performance. *ACS Nano* **2012**, *6*, 4713−4721.
(26) Du, G.; Guo, Z.; Wang, S.; Zeng, R.; Chen, Z.; Liu, H. Superior Stability and High Capacity of Restacked Molybdenum Disulfide as Anode Material for Lithium Ion Batteries. *Chem. Commun.* **2010**, *46*, 1106−1108.
(27) Xiao, J.; Wang, X.; Yang, X. Q.; Xun, S.; Liu, G.; Koech, P. K.; Liu, J.; Lemmon, J. P. Electrochemically Induced High Capacity Displacement Reaction of PEO/MoS_2/graphene Nanocomposites with Lithium. *Adv. Funct. Mater.* **2011**, *21*, 2840−2846.
(28) Yersak, T. A.; Macpherson, H. A.; Kim, S. C.; Le, V. D.; Kang, C. S.; Son, S. B.; Kim, Y. H.; Trevey, J. E.; Oh, K. H.; Stoldt, C. Solid State Enabled Reversible Four Electron Storage. *Adv. Energy Mater.* **2013**, *3*, 120−127.
(29) Puthussery, J.; Seefeld, S.; Berry, N.; Gibbs, M.; Law, M. Colloidal Iron Pyrite (FeS_2) Nanocrystal Inks for Thin-Film Photovoltaics. *J. Am. Chem. Soc.* **2011**, *133*, 716−719.
(30) Hu, Z.; Zhang, K.; Zhu, Z.; Tao, Z.; Chen, J. FeS_2 Microspheres with an Ether-Based Electrolyte for High-Performance Rechargeable Lithium Batteries. *J. Mater. Chem. A* **2015**, *3*, 12898−12904.
(31) Hu, Z.; Zhu, Z.; Cheng, F.; Zhang, K.; Wang, J.; Chen, C.; Chen, J. Pyrite FeS_2 for High-Rate and Long-Life Rechargeable Sodium Batteries. *Energy Environ. Sci.* **2015**, *8*, 1309−1316.
(32) Hillebrand, W. The Vanadium Sulphide, Patronite, and Its Mineral Associates from Minasragra, Peru. *J. Am. Chem. Soc.* **1907**, *29*, 1019−1029.
(33) Allmann, R.; Baumann, I.; Kutoglu, A.; Rösch, H.; Hellner, E. Die Kristallstruktur des Patronits $V(S_2)_2$. *Naturwissenschaften* **1964**, *51*, 263−264.
(34) Rout, C. S.; Kim, B. H.; Xu, X.; Yang, J.; Jeong, H. Y.; Odkhuu, D.; Park, N.; Cho, J.; Shin, H. S. Synthesis and Characterization of Patronite Form of Vanadium Sulfide on Graphitic Layer. *J. Am. Chem. Soc.* **2013**, *135*, 8720−8725.
(35) Xu, X.; Jeong, S.; Rout, C. S.; Oh, P.; Ko, M.; Kim, H.; Kim, M. G.; Cao, R.; Shin, H. S.; Cho, J. Lithium Reaction Mechanism and High Rate Capability of VS_4-Graphene Nanocomposite as an Anode Material for Lithium Batteries. *J. Mater. Chem. A* **2014**, *2*, 10847−10853.
(36) Li, Q.; Sheng, J.; Wei, Q.; An, Q.; Wei, X.; Zhang, P.; Mai, L. A Unique Hollow Li_3VO_4/Carbon Nanotubes Composite Anode for High-Rate Long-Life Lithium-Ion Batteries. *Nanoscale* **2014**, *6*, 11072−11077.
(37) Zhang, C.; Mahmood, N.; Yin, H.; Liu, F.; Hou, Y. Synthesis of Phosphorus-Doped Graphene and Its Multifunctional Applications for Oxygen Reduction Reaction and Lithium Ion Batteries. *Adv. Mater.* **2013**, *25*, 4932−4937.
(38) Zheng, S.; Wen, Y.; Zhu, Y.; Han, Z.; Wang, J.; Yang, J.; Wang, C. In Situ Sulfur Reduction and Intercalation of Graphite Oxides for Li-S Battery Cathodes. *Adv. Energy Mater.* **2014**, *4*. 10.1002/aenm.201400482.
(39) Xie, X.; Ao, Z.; Su, D.; Zhang, J.; Wang, G. MoS_2/Graphene Composite Anodes with Enhanced Performance for Sodium-Ion Batteries: The Role of the Two-Dimensional Heterointerface. *Adv. Funct. Mater.* **2015**, *25*, 1393−1403.
(40) Li, Y.; Liang, Y.; Hernandez, F. C. R.; Yoo, H. D.; An, Q.; Yao, Y. Enhancing Sodium-Ion Battery Performance with Interlayer-Expanded MoS_2-PEO Nanocomposites. *Nano Energy* **2015**, *15*, 453−461.
(41) Zhang, S. S. The Redox Mechanism of FeS_2 in Non-Aqueous Electrolytes for Lithium and Sodium Batteries. *J. Mater. Chem. A* **2015**, *3*, 7689−7694.
(42) Qu, B.; Ma, C.; Ji, G.; Xu, C.; Xu, J.; Meng, Y. S.; Wang, T.; Lee, J. Y. Layered SnS_2-Reduced Graphene Oxide Composite−A High-Capacity, High-Rate, and Long-Cycle Life Sodium-Ion Battery Anode Material. *Adv. Mater.* **2014**, *26*, 3854−3859.
(43) Jiang, J.; Feng, Y.; Mahmood, N.; Liu, F.; Hou, Y. SnS_2/Graphene Composites: Excellent Anode Materials for Lithium Ion Battery and Photolysis Catalysts. *Sci. Adv. Mater.* **2013**, *5*, 1667−1675.
(44) Zhou, T.; Pang, W. K.; Zhang, C.; Yang, J.; Chen, Z.; Liu, H. K.; Guo, Z. Enhanced Sodium-Ion Battery Performance by Structural Phase Transition from Two-Dimensional Hexagonal-SnS_2 to Orthorhombic-SnS. *ACS Nano* **2014**, *8*, 8323−8333.
(45) Xin, S.; Yin, Y.; Guo, Y.; Wan, L. A High-Energy Room-Temperature Sodium-Sulfur Battery. *Adv. Mater.* **2014**, *26*, 1261−1265.
(46) Klepp, K.; Gabl, G. New Complex Sulfides of the Va-Metals: Preparation and Crystal Structure of Na_3VS_4 (with a Note on the Crystal Structure of the Low Temperature Modification of Na_3PO_4). *ChemInform* **1998**, *29*, no10.1002/chin.199820008
(47) Leising, R. A.; Takeuchi, E. S. Solid-State Cathode Materials for Lithium Batteries: Effect of Synthesis Temperature on the Physical and Electrochemical Properties of Silver Vanadium Oxide. *Chem. Mater.* **1993**, *5*, 738−742.

DOI: 10.1021/acsami.5b06385
ACS Appl. Mater. Interfaces 2015, 7, 20902−20908